Vibrational and Electronic Spectroscopy of the Fluorene Cation

Jan Szczepanski, John Banisaukas, and Martin Vala*

Department of Chemistry and Center for Chemical Physics, University of Florida, Gainesville, Florida 32611-7200

So Hirata and Rodney J. Bartlett

Quantum Theory Project, University of Florida, Gainesville, Florida 32611-8435

Martin Head-Gordon

Department of Chemistry, University of California and Chemical Sciences Division, Lawrence Berkeley National Laboratory, Berkeley, California 94720

Received: August 7, 2001; In Final Form: October 26, 2001

The fluorene cations, $C_{13}H_{10}^+$ and $C_{13}D_{10}^+$, have been formed by both electron impact ionization and vacuum ultraviolet photoionization, deposited in an argon matrix at 12K and studied via Fourier transform infrared and ultraviolet/visible absorption spectroscopy. Harmonic vibrational frequencies have been calculated using density functional theory (B3LYP/6-31G(d,p)) and vibrational band assignments made. Good agreement is found. Dramatic differences have been observed in the infrared band intensities of the cations compared to their neutral parents. Two excited electronic band systems have been observed and compared with previous photoelectron spectroscopic results. New calculations of the fluorene cation excited states have been performed using configuration interaction singles (CIS), CIS with a doubles correlation correction (CIS(D)), time-dependent Hartree−Fock (TDHF), and time-dependent density functional theory (TDDFT) with SVWN, BLYP, and B3LYP functionals. Theoretically, 12 low-lying excited states were found, six of which match closely with PES and optical band energies. Certain additional visible and IR bands, which appear only with higher electron impact ionization energies, are ascribed to the singly dehydrogenated neutral $C_{13}H_9$ ($C_{13}D_9$) fragment. TDDFT calculations on the excited states and B3LYP calculations of the infrared and Raman-active vibrations of the $C_{13}H_9$ ($C_{13}D_9$) product are consistent with this attribution. Evidence is presented for matrix-trapped cationic fragments, probably dehydrogenated species.

I. Introduction

Polycyclic aromatic hydrocarbons (PAHs) play a significant role in combustion processes as well as in interstellar chemistry.[1−6] In an environment of high-flux UV photons and/or electrons, most PAHs are expected to be ionized. Many ionic PAHs have now been studied using such different experimental techniques as optical and/or infrared matrix isolation spectroscopy (MIS),[7−13] ion cyclotron resonance mass spectrometry (ICR-MS),[14−17] photoelectron spectroscopy (PES),[18−19] and, recently, multiphoton photodissociation spectroscopy employing an infrared free electron laser.[20]

In the present paper, the ultraviolet, visible, and infrared absorption spectra of the fluorene cation ($C_{13}H_{10}^+$) and its perdeuterated partner ($C_{13}D_{10}^+$) are presented. Recent FTICR-MS and theoretical studies on the photodissociation of the fluorene cation have shown that fragmentation of the fluorene cation occurs via a number of different photoreaction pathways, the most efficient of which is the loss of one to five hydrogens.[15,16] Photodehydrogenation of the cation requires only ca. 2.7 eV energy to remove one of the two hydrogens from the sp^3carbon of the five-membered ring.[16,21] Interestingly, for the $C_{10}H_5^+$ species, four of the hydrogens removed come from one of the six-membered rings. The low-energy threshold for fragmentation of the fluorene cation is consistent with the observation of many fragment bands in the present matrix experiment. Special care was therefore needed to generate unfragmented fluorene cations.

Calculation of the electronic vertical excitation energies for fluorene cation and its fluorene-like fragments, $C_{13}H_9^+$, $C_{13}H_8^+$, $C_{13}H_7^+$, $C_{13}H_6^+$, $C_{13}H_5^+$, as well as a $C_{13}H_9$ fluorene neutral fragment, were performed using configuration interaction singles (CIS), CIS with a doubles correlation correction (CIS(D)), time-dependent Hartree−Fock (TDHF), and time-dependent density functional theory (TDDFT) using the SVWN, BLYP, and B3LYP levels. Harmonic vibrational frequencies of the fluorene cation in its electronic ground state were also calculated at the unrestricted DFT/B3LYP/6-31G(d, p) level of theory.

II. Computational Methods

The geometries of the fluorene radical cation and its dehydrogenated products were optimized using the DFT model employing the hybrid Becke3-Lee−Yang−Parr (B3LYP) functional[22] and the 6-31G (d,p) basis set. The optimized geometries showed planar carbon skeletons with the C_{2v} molecular symmetry (cf. Figure 1). The vertical excitation energies and oscillator strengths were computed by a series of single excitation theories, i.e., configuration interaction singles (CIS),[23] time-dependent Hartree−Fock (TDHF) (also known as the

* Corresponding author. E-mail: mvala@chem.ufl.edu.

10.1021/jp013059g CCC: $22.00
Published on Web 12/12/2001

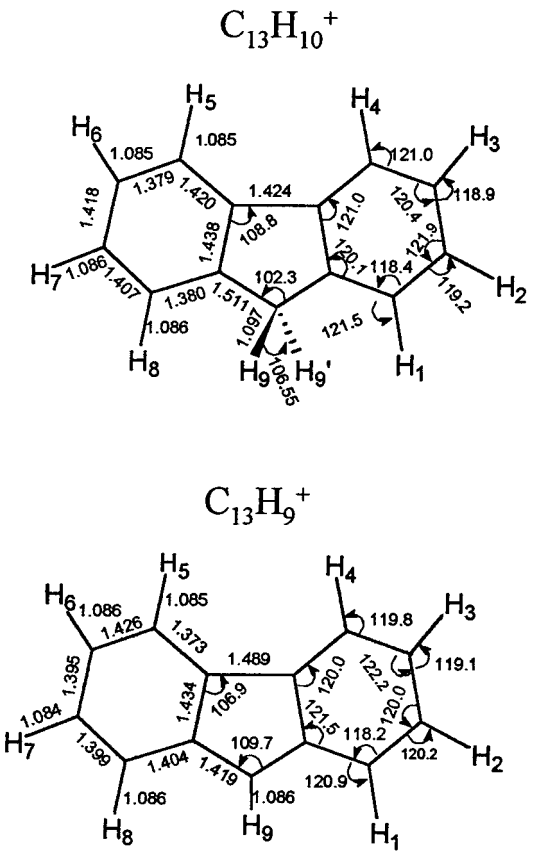

Figure 1. Optimized ground-state structures for the fluorene cation, $C_{13}H_{10}^+$, and its dehydrogenated cationic fragment, $C_{13}H_9^+$, calculated at the B3LYP/6-31G(d,p) level. The C−H$_9$ (or C−H$_{9'}$) bond energy in $C_{13}H_{10}^+$ cation (B3LYP/6-31G(d,p)) is only 2.7 eV. Adapted from ref 21.

"linearized" random-phase approximation or RPA), time-dependent density functional theory (TDDFT),[24,25] and CIS with a doubles correlation correction [CIS(D)].[26]

For the fluorene radical cation, spin-unrestricted CIS, TDHF, and TDDFT employing the Slater−Vosko−Wilk−Nusair (SVWN),[27,28] Becke-Lee−Yang−Parr (BLYP),[29,30] and B3LYP functionals were performed with the 6-31G(d, p) basis set. CIS and TDHF are among the simplest excited-state treatments for radicals, however, the errors in the calculated transition energies of simple radicals using these techniques can be in excess of several electronvolts.[31,32] TDDFT exhibits varied performance for radical excited states, depending on the character of the excited states.[33] For high-lying diffuse excited states and Rydberg excited states, in particular, with current approximate functionals, TDDFT substantially underestimates the excitation energies. This results from the nonphysical exponential decay of exchange-correlation potentials as opposed to the correct $-1/r$ asymptotic decay.[34,35] For low-lying excited valence states, TDDFT provides remarkably improved descriptions, relative to CIS or TDHF, for excited states including those that, when treated by the latter methods, can involve a significant fraction of double excitation character. The negative of the highest occupied Kohn−Sham (KS) orbital energy is a useful, albeit approximate, index that divides the full range of excitation energies into valence and Rydberg regions in the context of the performance of TDDFT.[34] Since this quantity for any PAH radical cation is very large (10.2 eV for the fluorene radical cation at BLYP/6-31G(d, p)) and all the excited states of interest to us are in the valence region, TDDFT is ideally suited for interpreting the electronic absorption spectra of the fluorene radical cation. For similarly sized PAH radical cations, an average accuracy of 0.3 eV for low-lying excited states has been found.[36] The computational cost of TDDFT calculations is comparable to that of CIS or TDHF calculations (see, e.g., ref 37 for TDDFT calculations of even larger PAH's).

For the sp^3-dehydrogenated fluorene cation, spin-restricted CIS, TDDFT employing SVWN, BLYP, and B3LYP functionals, and CIS(D) with the 6-31G(d,p) basis set were performed. The frozen core approximation was invoked for the CIS(D) calculation. The performance of TDDFT for closed-shell systems parallels that for open-shell systems.[38−41] The negative of the highest occupied orbital energy of this molecule is 9.6 eV (BLYP/6-31G(d, p)) and is again significantly higher than the transition energies to any of the excited states of interest to us. CIS generally provides adequate zeroth-order descriptions of closed-shell excited states, but it is not unusual to find errors of 0.5−1.0 eV or more in the calculated excitation energies. CIS(D) is roughly an excited-state analogue of second-order Møller−Plesset perturbation (MP2) theory and may also be viewed as a size-extensive approximation to equation-of-motion coupled-cluster singles and doubles (EOM-CCSD)[42−44] with reduced computational scaling. CIS(D) systematically diminishes the errors in CIS excitation energies by a factor of 2 or more, while the computational cost per state is not significantly more than for MP2 of the ground state.[26]

We also performed excitation energy calculations of a dehydrogenated fluorene neutral fragment at the spin-unrestricted CIS, TDHF, and TDDFT (SVWN, BLYP, and B3LYP) levels with the 6-31(2+, 2+)G(d,p) basis set. The basis set is considered to be flexible enough to describe some diffuse excited states of the neutral fragment. The negative of the highest occupied orbital energies are 4.7 (SVWN), 4.4 (BLYP), and 5.2 (B3LYP) eV, which are much lower than that of the fluorene cation or its cation fragments. In the following, therefore, we will confine our discussion to the calculated excitation energies below this energy threshold.

The basis set size requirement in TDDFT (and other single excitation theory calculations) for cations is expected to be modest, unlike for neutral or anion species. This is because the overall positive charges of the cations render their low-lying excited states much less diffuse than those of neutral or anionic species. The results of a TDDFT calculation of the fluorene radical cation, repeated at the BLYP/6-31++G(d, p) level, confirmed that the calculated excitation energies were within 0.03 eV of the corresponding BLYP/6-31G(d, p) results. Thus, the 6-31G(d, p) basis set employed in this study was considered to be sufficiently large for the cations examined in this study. Moreover, the B3LYP/6-31G(d,p) approach is reliable and inexpensive in predicting vibrational mode frequencies and relative integral intensities for medium size neutral and ionic PAHs in their electronic ground states. A generally good frequency match with experimental IR absorption bands has been reported, even using a lower basis set such as 4-31G.[45, 46]

All calculations were carried out with the Q-Chem quantum chemistry program[47]on IBM RS/6000 workstations. Further technical details of the methods employed in this study can be found in ref 47, as well as in refs 33 and 36 for TDDFT and in ref 26 for CIS(D).

III. Experimental Methods

In the present experiments, fluorene ($C_{13}H_{10}$, Sigma) or perdeuterated fluorene ($C_{13}D_{10}$, Cambridge Isotope Laboratories) was sublimed at 25−40 °C from a glass container into the cryostat vacuum deposition chamber. The fluorene vapor was

mixed with Ar gas and deposited on a cryostat window (CsI or BaF_2) cooled to 12−30 K by a closed-cycle helium refrigerator (Displex ADP).

Two ionization techniques were employed: either low energy electron ionization (EI) or vacuum UV photon ionization (PI). In the EI procedure, electrons from the hot cathode of the electron gun, accelerated by the 50−300 V cathode-to-anode electric field, interact with fluorene molecules or Ar atoms in a crossed beam configuration. An additional O-ring electrode (at +70 V), located just before the front cryostat window, provides an electrical field in the ionization region which attracts electrons from the electron gun as well as secondary electrons released from ionization events. With ca. 10^{-5} Torr pressure in the ionization region, the secondary electron current was 40−50 times higher than the current of electrons emitted directly from the electron gun. Since the concentration ratio of [Ar]/[$C_{13}H_{10}$] was ca. 1000, the predominant ion expected was Ar^+. This implies a relatively high fluorene ionization yield either via charge transfer ($Ar^+ + C_{13}H_{10} \rightarrow Ar + C_{13}H_{10}^+$) or Penning ionization ($Ar^* + C_{13}H_{10} \rightarrow Ar + C_{13}H_{10}^+ + e^-$). To increase the fluorene cation yield, 0.1% CCl_4 was added to the Ar gas in the EI method. The CCl_4 electron impact products serve as scavengers of any free electrons that could neutralize fluorene cations in the matrix. In addition, the negative ions trapped in the matrix, such as Cl^-, act to balance the positive charge buildup during cation deposition.[7−10]

In the PI procedure, Lyman radiation (λ 121.6 nm, 10.2 eV) emitted by atomic hydrogen intersects the Ar/$C_{13}H_{10}$ beam and ionizes fluorene. Electronically excited atomic hydrogen was produced by microwave discharge (2.45 GHz, 50−100W) of a He:Ar:H_2 mixture (72%:20%:8%, 0.1 Torr). The discharge region was isolated from the cryostat chamber by a window (LiF) transparent to10.2 eV photons. Since the fluorene ionization energy is 7.9 eV,[48] the 2.3 eV (= 10.2−7.9 eV) excess energy is not sufficient to remove any hydrogens from the parent $C_{13}H_{10}^+$ species.

The fluorene cation production yield was higher for the EI method. Ionic band intensities were found to grow almost linearly with deposition time. With the PI method, the dependence of ion band intensities vs time was linear only for ca. 15 min, during which a thin matrix was formed. In the 1040−500 cm^{-1} region, where many CCl_4 neutral and ionic product bands could mask the fluorene cation spectrum, the PI method produced better quality spectra. Using the IR and UV/visible band intensity correlation procedure,[9,10] together with the two independent ionization methods, it was readily possible to identify the newly observed bands as belonging either to the fluorene cation or to its fragments.

The IR (5000−400 cm^{-1}) and UV/visible (220−900 nm) absorption spectra of neutral fluorene, its cation, and photofragments isolated in solid Ar were recorded using MIDAC FT-IR spectrometer (0.5 cm^{-1} resolution) and an IBM 9420 spectrophotometer (0.28 nm resolution), respectively, in an experimental setup that allowed spectra to be recorded on the same sample-matrix in the two energy regions.

IV. Results and Discussion

A. Vibrational Spectra. The experimental fluorene cation infrared absorption spectra are displayed in Figure 2 ($C_{13}H_{10}^+$) and Figure 3 ($C_{13}D_{10}^+$). The band frequencies and relative intensities are listed in Table 1. The spectra in Figure 2 a,b were recorded for two different electron gun energies: 200 eV (top spectrum) and 50 eV (bottom spectrum). Since secondary (and perhaps tertiary) electron collisions (with lower, albeit

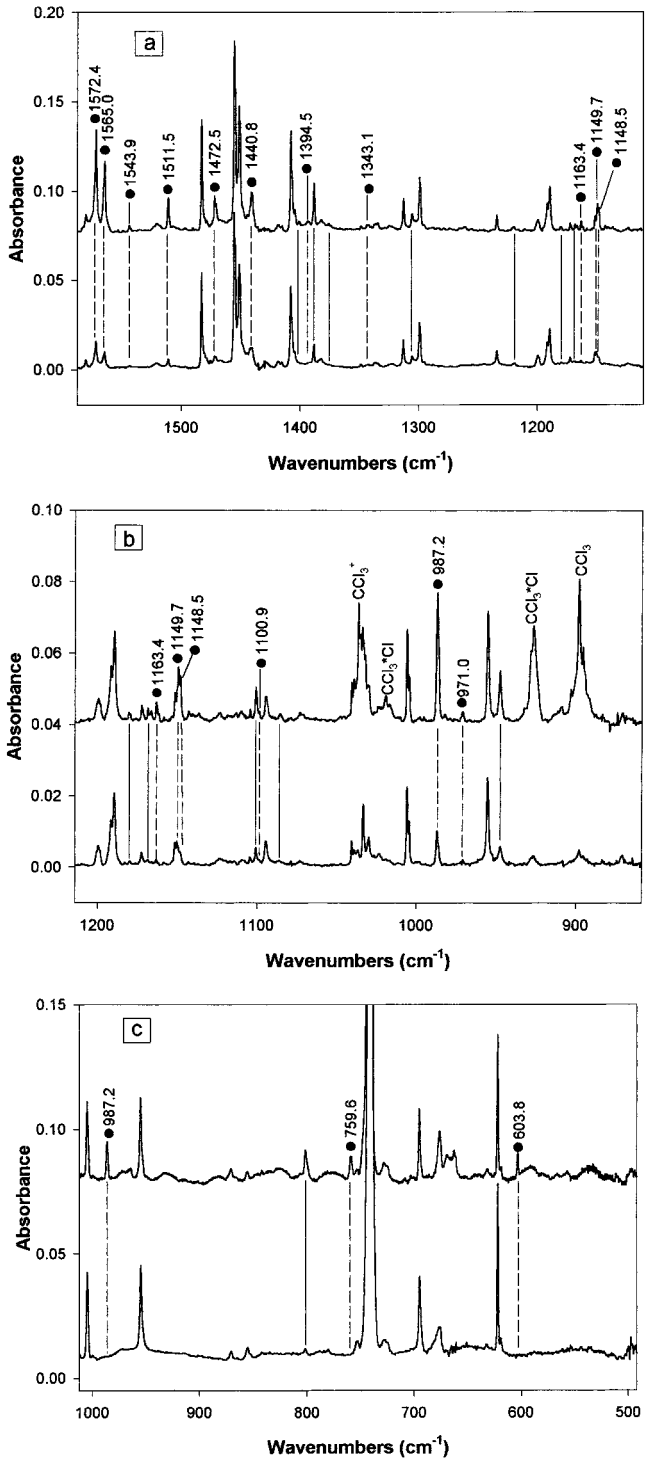

Figure 2. Infrared absorption spectra of neutral fluorene ($C_{13}H_{10}$), its cation and fragments isolated in solid Ar (12K) in three regions: (a) 1600−1150, (b) 1210−870, and (c) 1000−500 cm^{-1}. Spectra a and b were recorded using two different electron gun energies: 200 (upper spectrum) and 50 eV (lower spectrum). The electron impact product bands of CCl_4 are marked in spectrum b. The spectra in c were collected after ionization of fluorene using Lyman radiation. The bottom spectrum was recorded after matrix photolysis (1 h) with a 100W medium-pressure Hg lamp, while the upper spectrum was recorded on an unphotolyzed matrix. The bands due to fluorene cations are marked with dots and dashed vertical lines, while the positions of fluorene fragment bands are indicated by solid vertical lines. Note the faster decline of the cationic band intensities during photolysis for matrices prepared with Lyman radiation than with the electron impact ionization technique (cf. Figure 3).

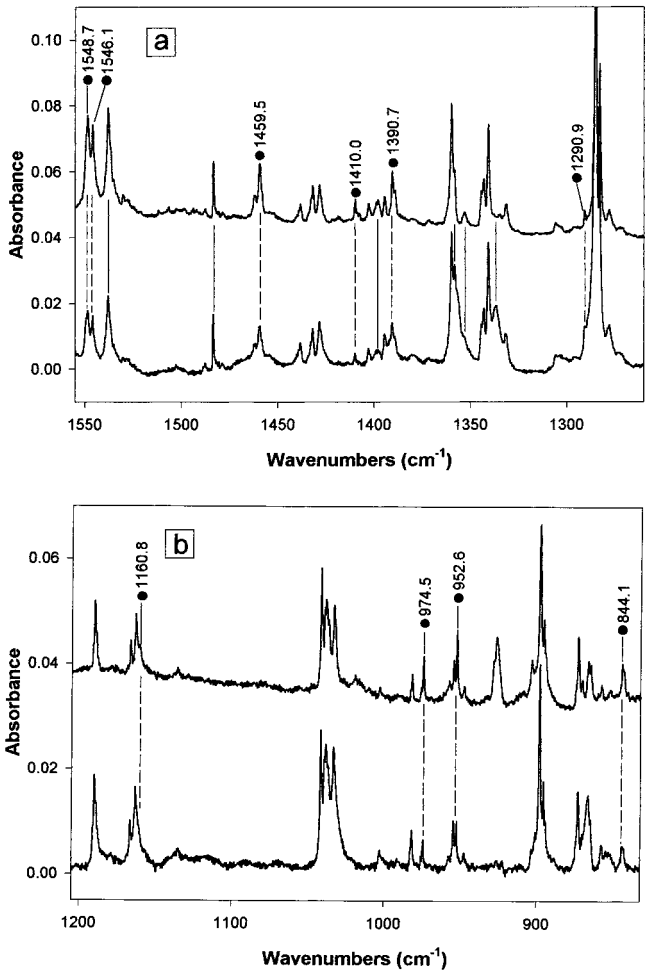

Figure 3. Infrared absorption spectrum of perdeuterated fluorene ($C_{13}D_{10}$) and its cation isolated in solid Ar (12K, 0.1%CCl_4 added) in the 1550−1250 cm^{-1} (Figure 3a) and 1200−840 cm^{-1} regions (Figure 3b). The lower spectrum was recorded after matrix photolysis (for 9 h) using the full output of a 100W medium-pressure Hg lamp. The $C_{13}D_{10}^+$ bands are marked by dots and dashed vertical lines, while the fragment bands are indicated by solid vertical lines. Unmarked bands are due to neutral $C_{13}D_{10}$.

unknown, energies) are more frequent than first-impact electron ionization processes, it is expected that with 200 eV electron energies, ionization events would be more numerous than with 50 eV electron energies. In fact, the electron beam current crossing a fluorene/Ar beam was ca. twice as large for 200 eV as that for 50 eV electron beam energies (55 μA vs 25 μA, respectively, as monitored by the O-ring electrode). Therefore, the yield of ionized fluorene is expected to be greater for higher electron beam energies. As shown in Figure 2a,b, higher band intensity ratios (fluorene cation/fluorene neutral) are observed in the 200 eV, compared to the 50 eV, spectrum.

The spectra in Figure 2c were obtained using the PI method and recorded before photolysis (top spectrum) and after matrix photolysis for 1 h (bottom spectrum). The IR spectra of $C_{13}D_{10}^+$ ion (cf. Figure 3a,b) were recorded using the EI method, while the bottom spectrum was collected after photolysis (9 h) using the full output from a medium-pressure Hg lamp (100W). It is well-known that during such photolyses, electrons are liberated from anions in the matrix via photodetachment and act to maintain the matrix charge balance.[8−10] The free electrons can be readily trapped by either the fluorene or other cations. Consequently, a decline in the concentration of cations is expected during photolysis. Photodissociation processes of cations trapped in the matrix could also deplete their concentrations. For all PAH cations studied thus far by us, except for the naphthalene cation, a depletion of ion concentration was observed with photolysis time. In the naphthalene cation case, Hg lamp photolysis resulted in a net gain of naphthalene cations because a two-step photoionization process involving a very long-lived triplet state ($\tau_{T1} > 2$ s) competes with the naphthalene cation electron capture process.

A greater decrease of fluorene cation concentration was observed during Hg lamp photolysis in the PI experiments than in the EI experiments (compare Figure 2c with Figure 3 spectra before and after photolysis). This phenomenon may be explained by the expected different spatial distribution of positive vs negative charges in the matrices for these two ionization techniques. For the PI method, the electrons ejected from fluorene by Lyman photolysis are recaptured by the closest X species forming a long-range $C_{13}H_{10}^+\cdots X^-$ pair. On the other hand, for the EI case, the $C_{13}H_{10}^+$ are created in the gas phase and deposited on the matrix surface together with electrons and X^- anions more uniformly, with the average distance of $C_{13}H_{10}^+$ to X^- larger than in the PI method. This implies a higher recapture probability of photodetached electrons from X^- anions by $C_{13}H_{10}^+$ during UV photolysis. Therefore, the higher rate of $C_{13}H_{10}^+$ concentration depletion is expected during Hg lamp photolysis for PI ionization method.

Geometry optimization (B3LYP/6-31G(d,p) level) for the ground state of neutral and cationic fluorene shows that the carbon framework is planar except for the two hydrogens on the sp^3 carbon which are aligned in a plane perpendicular to the mainframe (cf. Figure 1).[21] The calculated frequencies and intensities for $C_{13}H_{10}^+$ and $C_{13}D_{10}^+$ are given in Table 1, and a pictorial comparison of calculated and experimental spectra is shown in Figure 4.

The usual common factor (0.978) for this level of calculation was used to scale the calculated harmonic frequencies.[21] This factor brings the in-plane CCC bending vibration at 603.5 cm^{-1} and the out-of-plane C−H bending modes at 759.2 and 971.5 cm^{-1} into very good agreement with experiment (cf. Table 1). All calculated frequencies, excluding the C−H stretching modes (not observed), show an error compared to the experimental value of less than 23 cm^{-1} and an average error of 9.7 cm^{-1}. The same scaling factor was used to scale the calculated harmonic frequencies of $C_{13}D_{10}^+$. As Table 1 shows, the maximum error in the calculated frequencies is 15.3 cm^{-1}, while the average error is only 7.8 cm^{-1}

The 1572.5/1565.0 and 1548.7/1546.1 cm^{-1} doublets in the experimental spectrum of $C_{13}H_{10}^+$ (Figure 2a) and $C_{13}D_{10}^+$ (Figure 3a), respectively, are here assigned to the most intense C−C stretching vibration with a calculated integral intensity of 430 km/mol (cf. Table 1). Different matrix sites could generate the observed energy band splittings of 7.5 and 2.6 cm^{-1}, respectively. A similar band splitting of 2.0/5.0 cm^{-1} has been observed for a similar R(CC) mode of pyrene-h_{10}/pyrene-d_{10} cations in an Ar matrix.[49]

The experimental ν_H/ν_D frequency ratios for the strongest CC mode are consistent with the predicted ratio (of 1.02) from B3LYP/6-31(d,p) theory. Because this value is just over 1.0, a marginal contribution of the C−H (or C−D) vibration to the C−C stretching mode is indicated. Of the many PAH cations studied experimentally thus far, most have the same type of intense mode in the IR absorption spectrum, while for neutral PAHs the C−H out-of-plane bending and C−H stretching modes are the strongest.[8−13] Table 1 shows that the experimental values of the ν_H/ν_D ratio for the lower frequency modes are in

TABLE 1: Comparison of Observed (Ar matrix, 12K) and Calculated (B3LYP/6-31G(d,p)) Infrared Absorption Band Frequencies and Intensities for the Fluorene Cation ($C_{13}H_{10}^+$) and Perdeuterated Fluorene Cation ($C_{13}D_{10}^+$)[a]

mode description	$C_{13}H_{10}^+$		$C_{13}D_{10}^+$		ν_H/ν_D freq. ratio	
	calc. freq.[b]/cm^{-1}	obs. freq./cm^{-1}	calc. freq.[b]/cm^{-1}	obs. freq./cm^{-1}	calc.	obs.
τ(CCC)+ ϵ*(CH)*, b_1	225.3[6](0.01)		191.6(0.01)		1.18	
α(CCC)+ β*(CH)*, b_1	429.9[6](0.01)		372.2(0.01)		1.15	
α(CCC)+ β*(CH)*, b_2	603.5[32](0.07)	603.8(0.13)	583.0(0.07)		1.13	
ϵ(CH)+ τ(CCC), b_1	650.3[11](0.03)		535.0(0.06)		1.21	
ϵ(CH)+ τ(CCC), b_1	759.2[86](0.20)	759.6(0.19)	628.9(0.05)		1.20	
ϵ(CH)+ τ(CCC), b_1	971.5[5](0.01)	971.0(0.03)	822.2(0.00)		1.18	
ϵ(CH)+ τ(CCC), b_2	981.8[74](0.17)	987.2(0.35)	811.9(0.00)		1.21	
β(CH)+ R(CC), b_2	1006.9[5](0.01)	844.6(0.04)	844.1(0.10)		1.19	
β(CH)+ R(CC), b_2	1107.4[9](0.02)	1100.9(0.02)	857.2(0.01)		1.29	
β(CH)+ R(CC), b_2	1148.4[57] (0.13)	1149.7(0.15)	956.7(0.09)	952.6(0.19)	1.20	1.21
β(CH)+ R(CC), b_2	1167.0[1](0.00)	1163.4(0.05)	961.8(0.04)	974.5(0.16)	1.21	1.19
β(CH)+ R(CC), b_2	1204.5[6](0.01)		1027.0(0.03)		1.17	
β(CH)+ R(CC), b_2	1314.8[1](0.00)	1343.1(0.02)	1155.3(0.07)	1160.8(0.02)	1.14	1.16
R(CC)+ β(CH), b_2	1368.6[1](0.00)	1394.5(0.02)	1280.0(0.04)	1290.9(0.08)	1.07	1.08
R(CC)+ β(CH), a_1	1417.9[44](0.10)	1440.8(0.12)	1296.3(0.01)		1.09	
R(CC), a_1	1444.9[23](0.05)	1442.4(0.05)	1403.0(0.16)	1390.7(0.27)	1.03	1.04
R(CC), b_2	1464.6[35](0.08)	1472.5(0.14)	1410.4(0.07)	1410.0(0.12)	1.04	1.04
R(CC), a_1	1486.0[7](0.02)		1421.7(0.00)		1.05	
R(CC), b_2	1515.1[26](0.06)	1511.5(0.14)	1444.2(0.07)	1459.5(0.30)	1.05	1.04
R(CC), a_1	1542.3[13](0.03)	1543.9(0.03)	1497.9(0.03)		1.03	
R(CC), b_2	1587.5[430](1.0)	1572.4(1.0)[c]	1553.7((1.0)	1548.7(1.0)[d]	1.02	1.02

[a] The integral intensities (in km/mol) are given in brackets, while relative intensities are given in parentheses. Only bands of $C_{13}H_{10}^+$ with calculated intensities of 5 km/mol or larger are listed. The C−H stretching vibration frequencies around 3050 cm^{-1} are not listed since the intensity of the most intense band in this group is only 0.7 km/mol. Notation used: *R* are stretching vibration modes, α and β are in-plane bending vibration modes, and ϵ and τ are out-of-plane vibration modes. The first vibration indicated, in modes of mixed character, contributes the largest amount to the total vibration. The mode symmetries in C_{2v} point group are given in second column. [b] Frequencies scaled uniformly by 0.978 factor. [c] Intensity of the sum of 1572.4 and 1565.0 cm^{-1} doublet band. [d] Intensity of the sum of 1548.7 and 1546.1 cm^{-1} doublet band.

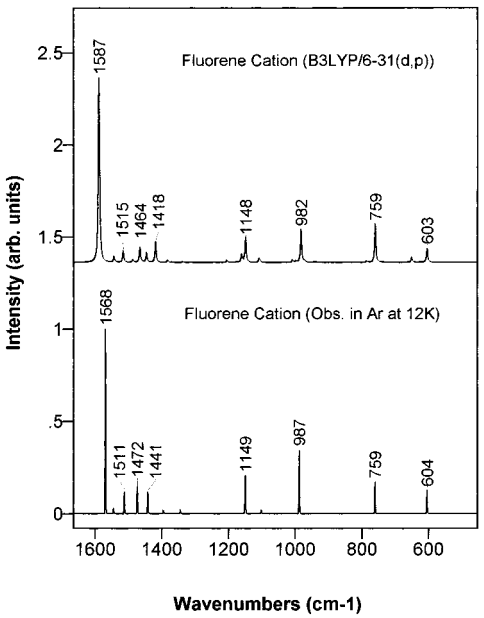

Figure 4. Calculated infrared absorption spectrum of $C_{13}H_{10}^+$ (upper panel) using unrestricted B3LYP/6-31G(d, p) level (0.978 frequency scale factor) and experimental spectrum of $C_{13}H_{10}^+$ (bottom panel). The bottom panel shows a "synthetic" spectrum created from experimental bands (dotted bands in Figure 2a−c) that were extracted with exact frequencies and intensities ratios. The observed close-lying doublets at 1472.5/1471.3 and 1572.4/1565.0 cm^{-1} are displayed here, with their intensities added for comparison purposes, as the 1472 and 1568 cm^{-1} bands, respectively.

good agreement with calculated ones indicating a larger contribution of C−H or C−D character to the C−C modes. This agreement strongly supports the experimental band assignments.

The calculated integral intensities of the C−H (C−D) stretching modes for the $C_{13}H_{10}^+$ ($C_{13}D_{10}^+$) ion are below 0.7 km/mol (3 km/mol). Thus, bands with an ionic signature were neither expected nor observed in the 3100−2900 cm^{-1} (2350−2240 cm^{-1}) region. There is a dramatic difference in the intensity distributions in the vibrational bands of the neutral and cationic fluorene. Such a difference has been noted earlier in studies on PAHs containing only six-membered rings.[8−13] Compared to neutral fluorene, the total integral intensity of the C−H stretching modes (3150−3000 cm^{-1} region) of the fluorene cation are ca. 100 times lower, whereas the C−C stretching modes (1610−1380 cm^{-1} region) are 20 times higher, the C−H in-plane bending modes (1250−1000 cm^{-1} region) are 14 times greater and the total intensity for the C−H out-of-plane modes (900−700 cm^{-1} region) remain practically unchanged.

B. Electronic Spectra. The optical absorption spectra for the fluorene cation ($C_{13}H_{10}^+$) and the perdeuterated cation ($C_{13}D_{10}^+$) in Ar (12K) are shown in Figure 5. Two band systems (commencing at ∼640 and ∼370 nm) can be seen. These transition energies are consistent with excited electronic state energies determined by Maier and Turner[18] and by Ruščić and co-workers,[50] using photoelectron spectroscopic (PES) methods. The PES values, together with the optical band positions, are listed in Table 2. There is good agreement between the values for the first optical transition (640 nm, 1.93 eV), however, the values for the second transition differ by 0.3 eV, possibly due to the difference in phase in the two experiments.[51]

Vertical excitation energies of the fluorene radical cation were calculated using the CIS, TDHF, and TDDFT approaches and are given in Table 2. A comparison of the computed values with the experimental ones reveals several interesting facts. First, neither the excitation energies nor intensities predicted from CIS and TDHF theory match the experimental results well. This was, however, expected, as described above, because HF-based single excitation theories are generally not capable of providing even the zeroth-order description of the low-lying excited states of radicals.[31,32] This is due to the fact that when treated by the HF-based theories, the ground-state wave functions of radicals

TABLE 2: Vertical Excitation Energies (in eV) and Oscillator Strengths (in Parentheses; "ia" Stands for Inactive) of the Fluorene Radical Cation Calculated by Spin-Unrestricted CIS, TDHF, and TDDFT Employing the SVWN, BLYP, and B3LYP Functionals with the 6-31G(d,p) Basis Set[a]

			TDDFT			
state	CIS	TDHF	SVWN	BLYP	B3LYP	experiment
$^2B_2$ ($\pi_0 \leftarrow \pi_{-1}$)	3.04 (0.1543)	2.38 (0.4671)	0.82 (0.0001)	0.89 (0.0002)	1.12 (0.0009)	0.86[b]
$^2A_2$ ($\pi_0 \leftarrow \pi_{-2}$)	3.32 (0.0002)	2.94 (0.0000)	1.10 (0.0004)	1.12 (0.0004)	1.34 (0.0007)	1.18[b]
$^2B_2$ ($\pi_0 \leftarrow \pi_{-3}$)	3.46 (0.2575)	3.05 (0.1600)	2.23 (0.1222)	2.19 (0.1196)	2.24 (0.1536)	1.93[b], 1.96[c], 1.93[d]
$^2B_1$ ($\pi_0 \leftarrow \sigma_{-1}$)	5.79 (0.0000)	5.72 (0.0000)	2.53 (0.0000)	2.79 (0.0000)	3.36 (0.0000)	3.13[b,e]
$^2A_1$ ($\pi_0 \leftarrow \sigma_{-2}$)	5.80 (ia)	5.66 (ia)	2.68 (ia)	2.95 (ia)	3.50 (ia)	
$^2B_1$ ($\pi_0 \leftarrow \sigma_{-3}$)	6.67 (0.0014)	6.58 (0.0015)	3.07 (0.0001)	3.34 (0.0001)	3.96 (0.0002)	
$^2A_1$ ($\pi_0 \leftarrow \sigma_{-4}$)	6.66 (ia)	6.58 (ia)	3.15 (ia)	3.42 (ia)	4.04 (ia)	
$^2A_2$ ($\pi_0 \leftarrow \pi_{-4}$)	5.04 (0.0243)	5.20 (0.0002)	3.51 (0.0001)	3.47 (0.0002)	3.75 (0.0003)	
$^2B_2$ ($\pi_1 \leftarrow \pi_0$)	4.47 (0.1160)	3.63 (0.0109)	3.97 (0.2857)	3.70 (0.2002)	3.77 (0.2968)	3.64[b], 3.35[d]
$^2A_2$ ($\pi_1 \leftarrow \pi_{-1}$)	5.17 (0.1229)	4.92 (0.1182)	3.91 (0.0016)	3.88 (0.0028)	4.17 (0.0063)	
$^2B_2$ ($\pi_0 \leftarrow \pi_{-5}$)	7.26 (0.3304)	7.03 (0.3617)	3.69 (0.0675)	3.89 (0.1180)	4.13 (0.0041)	4.08[b]
$^2B_2$ ($\pi_1 \leftarrow \pi_{-2}$)	5.22 (0.0055)	4.87 (0.0003)	4.16 (0.0025)	4.09 (0.0035)	4.40 (0.0001)	

[a] The geometry is optimized at the B3LYP/6-31G(d,p) level. The carbon skeleton lies in the *xz* plane with the longer molecular axis parallel to the *x* axis. The ground-state wave function transforms as $^2A_2$ irreducible representation in C_{2v} symmetry. The π and σ orbitals are numbered in the order of increasing orbital energies. The π_{-1}, π_0, and π_1 denote the highest doubly occupied, the singly occupied, and the lowest unoccupied π orbitals, respectively. [b] Photoelectron data, ref 50. [c] Gas-phase data for $C_{13}H_{10}^+ \cdot Ar$ complex, ref 53. [d] The present study. [e] The onset of a σ-electron ionization manifold.

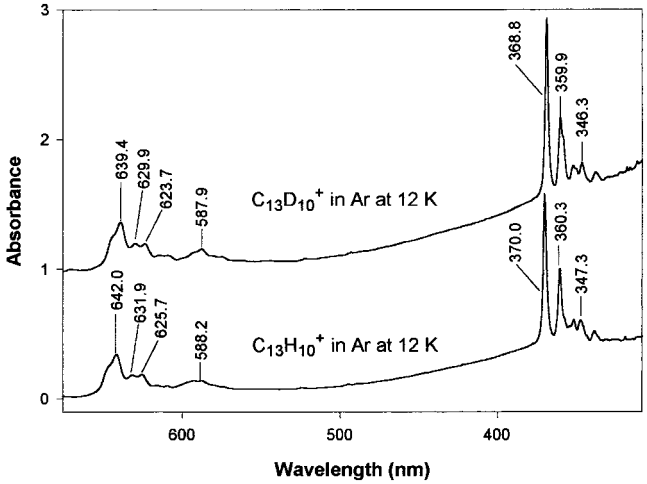

Figure 5. Electronic absorption spectra for fluorene cation, $C_{13}H_{10}^+$ (bottom spectrum), and for fully deuterated fluorene cation, $C_{13}D_{10}^+$ (upper spectrum), both isolated in solid Ar at 12K. The ions were generated using electron ionization method (see text). Note the ca. 2.5 and 1.0 nm blue energy shifts for the $C_{13}D_{10}^+$ vs $C_{13}H_{10}^+$ bands in the red ($^2B_2$ (D_3) $\leftarrow$ $^2A_2$ (D_0)) transition and in the violet ($^2B_2$(D_k) $\leftarrow$ $^2A_2$-(D_0)) transition, respectively.

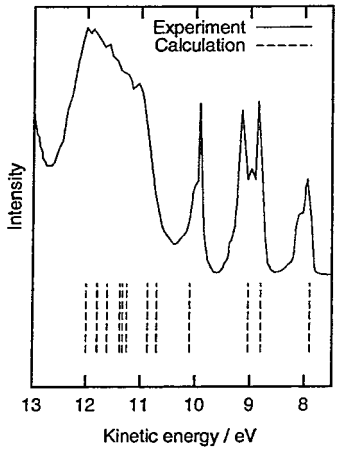

Figure 6. Calculated and observed photoelectron spectrum of fluorene. The calculated peak positions are obtained by adding the experimental first ionization potential of fluorene (7.91 eV) and the vertical excitation energies of fluorene radical cations computed by TDDFT employing the BLYP functional and 6-31G(d, p) basis set.

assume substantial multi-determinantal character. Also, many excitations also involve two-electron character and are beyond the applicability of single excitation theories such as CIS and TDHF.

A dramatic improvement in the calculated spectrum is accomplished, however, in going from HF-based single excitation theories to DFT-based single excitation theories. Now the excitation energies and intensities obtained from TDDFT are consistent with the experimental results, and it is straightforward to interpret the latter in terms of the calculated results. For example, TDDFT (BLYP/6-31G(d,p)) predicts three intense optical absorption bands in the energy range considered in Table 2. They are the transitions to 2 $^2B_2$ (2.19 eV), 3 $^2B_2$ (3.70 eV), and 4 $^2B_2$ (3.89 eV) excited states. The band at 1.93 eV (642 nm) in the electronic absorption spectrum and the sharp peak in the photoelectron spectrum[50] at 1.93 eV (relative to the transition to the cation ground state at 7.91 eV) can thus be unambiguously assigned to the first of these calculated transitions. The intense band at 3.35 eV (370 nm) in the optical absorption spectrum, whose counterpart in the photoelectron spectrum may be a small feature at 3.64 eV (= 11.55−7.91 eV) barely visible in a broad α-electron ionization manifold, is identified as the second of these transitions. The peak at 4.08 eV (= 11.99−7.91 eV) in the photoelectron spectrum may be assigned to the third of these transitions. Furthermore, the two sharp peaks at 0.86 eV (= 8.77−7.91 eV) and 1.18 eV (= 9.09−7.91 eV) in the photoelectron spectrum are reproduced well by the TDDFT calculations (0.89 and 1.12 eV). The fact that they are not observed in the electronic absorption spectrum is consistent with their negligibly small computed oscillator strengths.

The TDDFT calculation predicts that, besides these $\pi^* \leftarrow \pi$ transitions, there are several $\pi^* \leftarrow \sigma$ transitions in the 3−4-eV region, which are virtually invisible in the optical spectrum, but may give rise to bands associated with vibrational progressions in the photoelectron spectrum. Accordingly, we find a dense σ-electron ionization manifold in the 3−4 eV region (relative to the 7.91-eV peak) of the photoelectron spectrum. The onset of this σ-electron ionization manifold at 3.13 eV is, therefore, assigned to the transition to 1^2B_1. In Figure 6, we compare the vertical excitation energies of fluorene radical

TABLE 3: Band Assignments for the Electronic Absorption Spectrum of the Fluorene Cation, $C_{13}H_{10}^+$ and $C_{13}D_{10}^+$ (D_3 ($^2B_2$) ← D_0($^2A_2$) Transition), Observed in Ar Matrix at 12 K[a]

$C_{13}H_{10}^+$			$C_{13}D_{10}^+$			ν_H/ν_D freq. ratio	
obs. band/ nm	band assignment/ cm^{-1}	calc. freq./ cm^{-1}	obs. band/ nm	band assignment/ cm^{-1}	calc. freq./ cm^{-1}	obs.	calc.
642.0	0−0 trans.		639.4	0−0 trans.			
631.9	∼249[b]	215	629.9	∼236[b]	200	∼1.06	1.08
625.7	406	413	623.7	393	398	1.03	1.04
617.0	631(249+406)		614.7	628(236+393)			
609.6	828(2 × 406)		608.9	783(2 × 393)			
592.6	1299	1337	∼593.0	∼1224	1211	∼1.06	1.10
588.2	1425	1486	587.8	1373	1423	1.04	1.04
580.7	1651(249+1425)		580.9	1573(236+1373)			
574.6	1827(406+1425)		574.85	1754(393+1373)			

[a] All calculated (B3LYP/6-31G(d,p) level) a_1 symmetry (Raman-active) mode frequencies (cm^{-1}) of the $^2A_2$ electronic ground state are scaled by a factor of 0.978. [b] Overlapped by a fragment band (cf. Figure 8).

cation computed by TDDFT at the BLYP/6-31G(d,p) level and the photoelectron spectrum reported in ref 50. The calculated photoelectron peaks were obtained by adding the calculated excitation energies with the experimental first ionization potential of 7.91 eV. The geometry difference between the radical cation (on which the calculation is based) and the neutral molecule (for which the photoelectron spectrum is measured) was neglected. This comparison indicates that such an effect is marginal and the calculation reproduces the positions of all the principal peaks below 10.5 eV with quantitative accuracy. The dense σ ionization manifold commencing at 11 eV also coincides with the $\pi^* \leftarrow \sigma$ and $\pi^* \leftarrow \pi$ transitions. The capability of describing $\pi^* \leftarrow \sigma$ as well as $\pi^* \leftarrow \pi$ transitions in an unbiased manner is one of the desirable features of TDDFT, which may be missing in some multireference CI or perturbation theories.

The excitation energies exhibit slight variation with the exchange-correlation functionals employed. Overall, however, TDDFT reproduces the experimental excitation energies of the fluorene radical cation roughly within 0.3 eV and gives qualitatively correct intensity profiles.

The electronic absorption spectrum of fluorene cations in butyl chloride (77K) has been reported previously by Shida.[52] Strong peaks at 663, 610, 378, 366, and 355 nm were observed. Because of the much smaller interaction expected for the fluorene cation with Ar in the present work, the 663 and 610 nm bands observed by Shida can be expected to correspond to Ar matrix bands at 642 and 588.2 nm, while the 378, 366, and 355 nm bands measured by Shida can be associated with the 370.0, 360.3, and 347.3 nm Ar matrix bands, respectively. Bréchignac and co-workers reported part of the electronic absorption spectra (650−560 nm region) of the gas phase complexes, fluorene cation *Ar and fluorene cation *Ar_2, and assigned the main origin peak at ∼632.9 nm as the $D_3 \leftarrow D_0$ transition, which is the same as our assignment above.[53] The same band system for the fluorene cation was also observed in a Ne matrix and a band at ∼636 nm assigned as the $D_3 \leftarrow D_0$ origin.[54]

Generally, vibrational progressions in an electronic absorption spectrum involve symmetric modes. Under certain conditions, the excited-state vibrational frequencies may match the ground-state Raman frequencies closely. Table 3 shows a comparison of the observed excited-state vibrational frequency intervals for the 642.0 nm band system ($^2B_2 \leftarrow {}^2A_2$ transition) and several a_1 symmetry (Raman-active) mode frequencies calculated (using B3LYP/6-31G(d,p)) for the fluorene cation's $^2A_2$ ground state. From the good agreement, it can be concluded that the geometry and vibrational force constants in the $^2B_2$ excited state are not much different than that in the $^2A_2$ ground state. However, for the higher energy $^2B_2$ excited state (370 nm), the comparison was not good, precluding any assignment of the excited state modes from the calculated ground state normal mode vibrations. This difference presumably arises because the former transition involves electron excitation from a doubly occupied bonding molecular orbital to the singly occupied bonding orbital, while the latter involves electronic excitation from the singly occupied bonding orbital to an antibonding orbital (cf. Table 2).

For the lower-energy $^2B_2 \leftarrow {}^2A_2$ transition of the $C_{13}D_{10}^+$ ion, the observed vibrational frequencies are shifted to lower values, as expected (cf. Table 3). The ν_H/ν_D ratio for the excited state vibrations are more scattered than the analogous modes in the ground electronic state (cf. Table 1). This is most likely due to the fact that some of the frequencies in the excited state are relatively distant from the calculated mode frequencies of the ground state.

In summary, 12 low-lying electronic excited states of the fluorene cation (five $^2B_2$, three $^2A_2$, two $^2A_1$ (inactive) and two $^2B_1$) have been determined from the CIS, TDHF and TDDFT calculations (cf. Table 2). They are spread over ca. 5 eV energy with two relatively strong optical transitions predicted: one at ca. 2.2 eV and another at ca. 3.8 eV, with oscillator strengths of ca. 0.15 and 0.28, respectively. The observed optical absorptions at 1.93 eV (642.0 nm) and 3.35 eV (370.0 nm) (cf. Figure 5) are assigned to the $^2B_2(D_3) \leftarrow {}^2A_2(D_0)$ and $^2B_2(D_9) \leftarrow {}^2A_2(D_0)$ transitions, respectively. The vibronic structure for this transition is defined by the bands at 631.9 (overlapped with fragment band), 625.7, 617.0, 609.6, 592.6, 588.2, 580.7, and 574.6 nm bands (cf. Figures 5, 7, and 8). These bands are built on the 642.0 nm origin band at intervals of 249, 406, 631, 828, 1299, 1425, 1651, and 1827 cm^{-1}, respectively. The corresponding fundamental a_1 symmetry (Raman active) mode frequencies calculated at B3LYP/6-31G(d,p) (0.978 scale factor) for fluorene cation in its electronic ground state are 215, 413, 1337, and 1486 cm^{-1} (cf. Table 3).

C. Fragmentation. Many bands have been observed in the present study in both the IR and visible regions, which appear to arise from carriers that are neither ionic nor neutral fluorene. Their band intensities grow with the energy of the ionizing electron beam. The samples scanned in the Figure 7 spectra were produced with two different electron beam energies, 50 eV (bottom spectrum) and 300 eV (top spectrum). In the 300 eV spectrum of Figure 7, many additional bands have appeared. The question then becomes, If these bands are not fluorene cation bands, what are they? Are they due to fluorene fragments? If so, which one(s)? To examine the nature of the carriers of these bands, the following experimental and calculation strategies were applied. (a) The UV−visible and IR absorption spectra

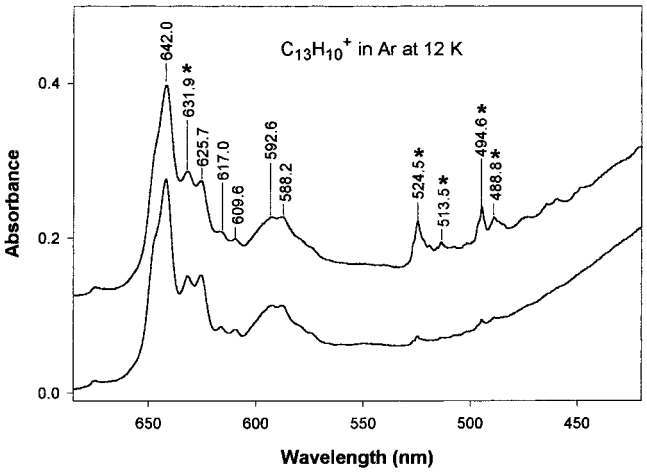

Figure 7. Part of the electronic absorption spectrum of fluorene cations ($C_{13}H_{10}^+$) deposited in solid Ar at 12K for two different electron gun energies: 50 (bottom spectrum) and 300 eV (upper spectrum). The starred bands at 631.9, 524.5, 513.5, 494.6, and 488.8 nm are due to different fluorene cation and neutral fragments (see text).

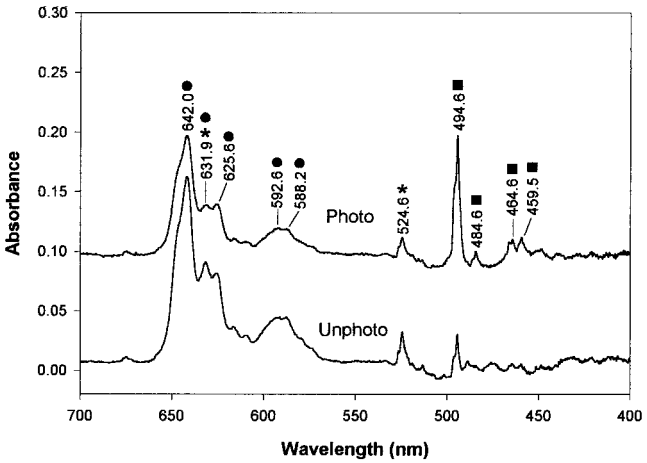

Figure 8. Photolysis effect on the matrix isolated fluorene cation and its fragments. The upper spectrum was recorded after 5 h matrix photolysis using 100W medium-pressure Hg lamp. The 494.6 nm band is assigned to the $^2A_2(D_2) \leftarrow {}^2B_2(D_0)$ 0−0 transition of $C_{13}H_9$ (one H off from sp^3 carbon of fluorene neutral) with the 418, 1227, 1315, and 1545 cm^{-1} vibration progression indicated by bands at 484.6 and 466.3 (not marked) and 464.6 and 459.5 nm (squares marked). The dotted bands are assigned to the $^2B_2(D_3) \leftarrow {}^2A_2(D_0)$ transition of the fluorene cation. The starred bands are due to different fluorene cation fragments.

were collected after extensive (16 h) UV photolysis of the $C_{13}H_{10}$/Ar matrix for the purpose of identifying the fluorene neutral fragments. (b) The 300 eV spectrum (and other spectra with an increased number of bands) was recorded in the visible and IR regions both before and after photolysis (Hg lamp). By using a band correlation approach, it was possible to classify some of the newly observed bands into different groups of fragment species. (c) The vertical excitation energies were calculated (TDDFT) for $C_{13}H_9$ fluorene neutral fragment as well as for $C_{13}H_9^+$, $C_{13}H_8^+$, $C_{13}H_7^+$, $C_{13}H_6^+$, and $C_{13}H_5^+$ fluorene-like ions and compared to the experimental spectra.

From the visible/IR spectra collected for no electron beam applied and different electron beam energies used on unphotolyzed/photolyzed sample matrices, the following conclusions can be drawn: (a) The 494.6, 484.6, 464.6, and 459.5 nm system bands (similar to those of Figure 8) are generated during UV photolysis of neutral fluorene in the Ar matrix. (b) The 631.9, 524.5, 513.5, 494.6, and 488.8 nm bands (Figure 7) do not arise from the fluorene neutral or cation. (c) From the visible/IR band intensity correlations, the 494.6 nm band shows a good intensity correlation with the 780.9 and 722.2 cm^{-1} infrared bands.

1. Singly Dehydrogenated Neutral $C_{13}H_9$ Species. The intensities of all the starred bands in Figures 7 and 8 (except for 494.6 nm) decrease during matrix photolysis. The intensity of the 494.6 nm band increases during photolysis (as do the bands at 484.6 and 466.3 (not marked) and 464.6 and 459.5 nm (cf. Figure 8)). The latter bands are at intervals of 418, 1227, 1315, and 1545 cm^{-1} from the 494.6 nm band and are assigned as vibrations built on the 494.6 nm origin. The identity of the carrier of this band system as the $C_{13}H_9$ fragment is consistent with the following results.

From the calculated C−H bond energies at B3LYP/6-31G-(d,p) level for fluorene neutral, it appears likely that the first hydrogen is removed from the sp^3 carbon. This process possesses no energy barrier and requires only 3.38 eV energy.

Second, the intensity of the 494.6 nm system bands correlates well (on matrix annealing and photolysis) with the intensity of infrared bands at 780.9 and 722.2 cm^{-1}. They have quite good energy coincidence to the 778.2 (52km/mol) and 724.9 (44km/mol) cm^{-1} (frequencies scaled by 0.978 factor), the two most intense vibrations in the calculated IR spectrum (B3LYP/6-31G-(d,p)) of singly dehydrogenated fluorene (sp^3 H removed).

Third, the UV photolysis (using a Hg lamp) of the fluorene/Ar matrix yielded a system of bands at 494.6 nm (similar to that in Figure 8 from electron impact) and ca. half as intense bands at 370.6 and 353.2 nm. To check the possibility that the 494.6, 370.6, and 353.2 nm bands are due to $C_{13}H_9$, we calculated the vertical excitation energies of sp^3-dehydrogenated $C_{13}H_9$ neutral fragment by CIS, TDHF, and TDDFT methods (compiled in Table 4). Again, we observe that the CIS and TDHF results differ substantially from the TDDFT results, and we dismiss the former results, as they cannot be considered qualitatively correct. The highest occupied orbital energies from the DFT calculations are in the range of 4.4 to 5.2 eV, and hence, the TDDFT excitation energies below 4 eV may be safely used for the assignment of the observed optical absorption bands. We find three principal absorption peaks below 4 eV in the BLYP/6-31(2+,2+)G(d,p) result: they are at 2.47 ($D_2 \leftarrow D_0$), 3.42 ($D_6 \leftarrow D_0$), and 3.58 ($D_7 \leftarrow D_0$) eV. The SVWN and B3LYP functionals also provide essentially the same spectra. The positions of these three peaks match closely the observed positions (2.51 (494.6), 3.34 (370.6), and 3.51 eV (353.2 nm)) of the photoinduced absorption features, and therefore, the assignment of these observed peaks to the $C_{13}H_9$ neutral fragment is tenable.

Fourth, the frequencies of the vibrational modes vibronically active in the 494.6 nm band system for the $C_{13}H_9$ and $C_{13}D_9$ fragments are matched quite well by the a_1 symmetry (Raman-active) mode frequencies calculated for the ground state of these species (cf. Table 5).

2. Singly Dehydrogenated $C_{13}H_9^+$ Cation. The photofragmentation of the fluorene cation, studied previously via ion cyclotron resonance measurements, showed that the main fragmentation channel is the loss of one to five hydrogens.[15,16] For the first H removed, the calculated (B3LYP/6-31G(d,p)) CH bond energy (sp^3 carbon) is only 2.7 eV.[21] Therefore, the dehydrogenation reactions of the fluorene cation are expected to also be active in our matrix ionization experiments.

Table 6 summarizes the vertical excitation energies calculated at CIS, TDDFT, and CIS(D) levels for such a $C_{13}H_9^+$ cation. For this closed-shell system, CIS appears to provide a qualitatively correct, but quantitatively deficient, description of several

TABLE 4: Vertical Excitation Energies (in eV) and Oscillator Strengths (in Parentheses; "ia" stands for inactive) of the sp³-Dehydrogenated Fluorene Neutral Radical Calculated by Spin-Unrestricted CIS, TDHF, and TDDFT Employing the SVWN, BLYP, and B3LYP Functionals with the 6−31(2+,2+)G(d,p) Basis Set[a]

			TDDFT			
state	CIS	TDHF	SVWN	BLYP	B3LYP	experiment
$^2A_2$ ($\pi_0 \leftarrow \pi_{-1}$)	4.11 (0.0122)	3.34 (0.0109)	1.46 (0.0002)	1.52 (0.0001)	1.74 (0.0006)	
$^2A_2$ ($\pi_0 \leftarrow \pi_{-2}$)	4.59 (0.0007)	4.43 (0.0040)	2.44 (0.0475)	2.47 (0.0462)	2.75 (0.0525)	2.51[b]
$^2B_2$ ($\pi_1 \leftarrow \pi_0$)	5.11 (0.0000)	4.21 (0.0003)	2.65 (0.0031)	2.69 (0.0031)	3.04 (0.0050)	
$^2B_2$ ($\pi_0 \leftarrow \pi_{-3}$)	5.38 (0.0006)	5.19 (0.0004)	3.10 (0.0011)	3.12 (0.0007)	3.50 (0.0000)	
$^2A_2$ ($\pi_1 \leftarrow \pi_{-1}$)	5.30 (0.1482)	5.09 (0.1088)	3.42 (0.0017)	3.31 (0.0016)	3.39 (0.0022)	
$^2B_2$ ($\pi_0 \leftarrow \pi_{-4}$)	5.66 (0.0018)	5.52 (0.0019)	3.45 (0.0155)	3.42 (0.0155)	3.69 (0.0153)	3.34[b]
$^2A_2$ ($\pi_2 \leftarrow \pi_0$)	5.68 (0.0036)	5.41 (0.0275)	3.57 (0.0298)	3.58 (0.0251)	3.93 (0.0359)	3.51[b]
$^2A_1$ ($\sigma_1 \leftarrow \pi_0$)	5.95 (0.0022)	5.95 (0.0020)	4.13 (0.0010)	3.80 (0.0009)	4.28 (0.0010)	
$^2B_1$ ($\sigma_2 \leftarrow \pi_0$)	5.54 (ia)	5.54 (ia)	4.32 (ia)	3.96 (ia)	4.51 (ia)	
$^2A_1$ ($\sigma_3 \leftarrow \pi_0$)	6.06 (0.0061)	6.06 (0.0059)	4.42 (0.0001)	4.05 (0.0002)	4.53 (0.0006)	
$^2A_1$ ($\pi_0 \leftarrow \sigma_{-1}$)	6.44 (0.0001)	6.44 (0.0001)	3.85 (0.0000)	4.12 (0.0000)	4.77 (0.0001)	
$^2A_2$ ($\pi_1 \leftarrow \pi_{-2}$)	6.04 (0.0273)	5.97 (0.0387)	4.33 (0.0179)	4.14 (0.0110)	4.37 (0.0154)	

[a] The geometry is optimized at the B3LYP/6-31G(d,p) level. The carbon skeleton lies in the *xz* plane with the longer molecular axis parallel to the *x* axis. The ground-state wave function transforms as $^2B_2$ irreducible representation in C_{2v} symmetry. [a]The π and σ orbitals are numbered in the order of increasing orbital energies. The π_{-1}, π_0, and π_1 denote the highest doubly occupied, the singly occupied, and the lowest unoccupied π orbitals, respectively. [b] The 494.6 (2.51), 370.6 (3.34) and 353.2 nm (3.51 eV) absorption bands observed in Ar matrix, present study.

TABLE 5: Band Assignments for the Electronic Absorption Spectrum of sp³-Dehydrogenated Fluorene Neutral, $C_{13}H_9$ and $C_{13}D_9$ ($^2A_2(D_2) \leftarrow {}^2B_2(D_0)$) Transition), Observed in Ar Matrix at 12K (cf. Figure 8)[a]

$C_{13}H_9$			$C_{13}D_9$			ν_H/ν_D freq. ratio	
obs. band/ nm	band assignment/ cm^{-1}	calc. freq./ cm^{-1}	obs. band/ nm	band assignment/ cm^{-1}	calc. freq./ cm^{-1}	obs.	calc.
494.6	0−0 trans.		492.9	0−0 trans.			
484.6	418	419	~483.1	~411	403	~1.02	1.04
466.3	1227	1192	*b*	*b*	1003	a	1.19
464.4	1315	1296	465.4	1199	1175	1.10	1.10
459.5	1545	1582	458.9	1503	1543	1.03	1.03

[a] All calculated (B3LYP/6-31G(d,p) level) a_1 symmetry (Raman-active) mode frequencies (cm^{-1}) of the $^2B_2$ electronic ground state are scaled by a factor of 0.978. [b] No band was identified possibly due to low S/N ratio.

TABLE 6: Vertical Excitation Energies (in eV) and Oscillator Strength (in Parentheses; "ia" Stands for Inactive) of the sp³-Dehydrogenated Fluorene Cation Calculated by Spin-Restricted CIS, CIS(D), and TDDFT Employing the SVWN, BLYP, and B3LYP Functionals with the 6-31G(d,p) Basis Set[a]

			TDDFT			
state	CIS	CIS(D)	SVWN	BLYP	B3LYP	experimental
$^1B_1$ ($\pi_1 \leftarrow \pi_{-1}$)	2.10 (0.0202)	1.40	1.25 (0.0007)	1.26 (0.0008)	1.37 (0.0022)	
$^1B_1$ ($\pi_1 \leftarrow \pi_{-2}$)	3.74 (0.5161)	2.59	2.67 (0.2016)	2.66 (0.2021)	2.83 (0.2597)	2.54[b]
$^1A_1$ ($\pi_1 \leftarrow \pi_{-3}$)	4.80 (0.0202)	3.52	2.98 (0.0068)	2.98 (0.0071)	3.34 (0.0087)	
$^1B_2$ ($\pi_1 \leftarrow \sigma_{-1}$)	6.33 (0.0002)	4.71	3.46 (0.0000)	3.68 (0.0000)	4.22 (0.0000)	
$^1A_2$ ($\pi_1 \leftarrow \sigma_{-2}$)	6.58 (ia)	5.13	3.60 (ia)	3.85 (ia)	4.44 (ia)	
$^1A_1$ ($\pi_1 \leftarrow \pi_{-4}$)	5.84 (0.2593)	4.69	3.91 (0.0362)	3.88 (0.0373)	4.29 (0.0623)	
$^1A_2$ ($\pi_1 \leftarrow \sigma_{-3}$)	7.31 (ia)	5.68	4.09 (ia)	4.33 (ia)	4.99 (ia)	
$^1B_2$ ($\pi_1 \leftarrow \sigma_{-4}$)	7.43 (0.0004)	5.88	4.15 (0.0001)	4.39 (0.0001)	5.07 (00002)	
$^1B_1$ ($\pi_1 \leftarrow \pi_{-5}$)	7.79 (0.0182)	5.54	4.54 (0.0485)	4.53 (0.0436)	5.17 (0.1062)	
$^1B_1$ ($\pi_2 \leftarrow \pi_{-1}$)	6.35 (1.5664)	5.45	4.79 (0.7120)	4.78 (0.7162)	5.07 (0.7054)	
$^1A_1$ ($\pi_3 \leftarrow \pi_{-1}$)	7.10 (0.0019)	5.92	5.05 (0.0491)	5.03 (0.0510)	5.54 (0.0896)	
$^1B_1$ ($\pi_2 \leftarrow \pi_{-2}$)	6.86 (0.0000)	6.05	5.23 (0.1285)	5.21 (0.1337)	5.68 (0.1421)	

[a] The geometry is optimized at the B3LYP/6-31G(d,p) level. The molecule lies in the *xz* plane with the longer molecular axis parallel to the *x* axis. The ground-state wave function transforms as $^1A_1$ irreducible representation of the C_{2v} symmetry. The π and σ orbitals are numbered in the order of increasing orbital energies. The π_{-1} and π_1 denote the highest doubly occupied and the lowest unoccupied π orbitals, respectively. [b] The 488.8 nm (2.54 eV) band in the optical absorption spectrum of the fragmented fluorene radical cation (cf. Figure 7), tentative assignment.

low-lying excited states. The TDDFT and CIS(D) results are consistent with each other. Based on previous tests of the CIS(D)[26] and TDDFT[36] approaches, we believe that the calculated excitation energy is within 0.3 eV of the experimental value.

An intense $\pi^* \leftarrow \pi$ transition is predicted at ~2.6 eV for the dehydrogenated (sp^3 H removed) fluorene cation species. TDDFT predicts that the transition energy to the most intense band of $C_{13}H_9^+$ cation fragment to be slightly higher than that of the $C_{13}H_9$ neutral fragment, which is also consistent with this assignment. Thus, the observed band at 488.8 nm (2.54 eV) (cf. Figure 7) is assigned tentatively to the S_2 ($^1B_1$) ← S_0 ($^1A_1$) transition of the $C_{13}H_9^+$ fragment species.

According to the calculations, the absolute intensities of these peaks are smaller, by 1 order of magnitude, than those of the most intense peaks of the cation fragments. In the measured spectrum, on the other hand, the photoinduced absorption bands assigned to the neutral fragment are ca. half as intense as those assigned to the cation fragments. Therefore, for our assignment to be correct, neutral fragments must be much more abundant than cation fragments when the optical absorption spectrum of the fluorene radical cation is measured. We consider this to be

quite likely in light of the much higher concentration of neutral versus cationic parent species from which these fragments are created.

3. Other Bands in the 525−450 nm Region. Vertical excitation energies for the $C_{13}H_n^+$ ($n = 5-8$) fluorene-like ion fragments, calculated via TDDFT (with SVWN, BLYP, and B3LYP functionals and a 6−31G(d,p) basis set) showed that the most intense transition in the visible region should lie at 2.66 eV (466 nm) to 2.71 eV (458 nm) for SVWN, 2.65 eV (467 nm) to 2.70 eV (459 nm) for BLYP, and 2.81 eV (441 nm) to 2.89 eV (429 nm) for B3LYP. Assuming that these values are overestimated by ca. 0.3 eV (cf. Tables 2, 4, and 6 and earlier discussion), the lowest energy limit for such a transition is 2.35 eV (527.6 nm). Therefore, the starred fragment bands in the 525−450 nm region of Figures 7 and 8 could be associated with one or more of those dehydrogenated fragments. However, given the similarity of the predicted excitation energies for these dehydrogenated fluorene fragments, it is not possible to be more conclusive with the present data.

Moreover, experimental[16] and theoretical[21] work on the gas-phase photofragmentation of the fluorene cation has demonstrated the formation of a variety of photoproducts, such as $C_5H_3^+$, C_7H^+, C_9^+, C_{11}^+, etc., for short photolysis times. Therefore, we cannot rule out more extensive fragmentation processes occurring through the proposed ring-opening mechanism.[21]

V. Conclusions

Fluorene, $C_{13}H_{10}$, and its perdeuterated partner, $C_{13}D_{10}$, were ionized by either low energy electron impact or vacuum UV photon ionization, deposited in argon matrices (12K), and scanned in the infrared and visible/ultraviolet regions. The observed infrared frequencies have been compared to frequencies calculated using density functional theory (B3LYP/6-31G(d,p)) with excellent agreement. Ratios (ν_H/ν_D) of the vibrational frequencies in $C_{13}H_{10}^+$ and $C_{13}D_{10}^+$ match well with calculated ratios and confirm the mode assignments. Dramatic differences are found in the intensity distributions of the fluorene cations and their neutral parents. The CH (CD) stretching modes are ca. 100 times less intense, the CC stretching modes are about 20 times more intense, and the CH (CD) in-plane bending modes are about 14 times more intense in the cationic species compared to the neutral species. The intensities of the CH (CD) out-of-plane vibrations remain practically unchanged.

Electronic absorption spectra of $C_{13}H_{10}^+$ and $C_{13}D_{10}^+$ were recorded in the visible and ultraviolet regions and revealed two band systems, one at ~640 nm and the other at ~370 nm. These transitions compare well with previous photoelectron spectroscopic results. Excitation energies of the fluorene radical cation were calculated using CIS, TDHF, and TDDFT approaches. Satisfactory agreement of the optical energies and the PES results with the TDDFT calculations (using different basis sets) has led to the assignments of the 640 and 370 nm optical bands to the D_3 ($^2B_2$) ← D_0 ($^2A_2$) and D_9 ($^2B_2$) ← D_0 ($^2A_2$) transitions, respectively. Of the twelve excited electronic states found in the calculations, six have been correlated with either PES energies and/or optical transitions.

Using electron impact ionization of fluorene, a number of new bands appear in the infrared and visible regions with higher electron gun energies. These bands do not belong to neutral or cationic fluorene. By a combination of experimental and theoretical procedures, it is shown that the 494.6 nm optical band and the 780.9 and 722.2 cm^{-1} infrared bands belong to the singly dehydrogenated fluorene fragment, $C_{13}H_9$. Confirmation was obtained by calculation of the a_1 symmetry (Raman-active) modes of $C_{13}H_9$ (and $C_{13}D_9$) which show a good match with the vibronic band intervals of the 494.6 nm optical absorption band system. Additional new bands are suggested to arise from products that are more fully dehydrogenated or deeply fragmented.

Acknowledgment. The authors wish to acknowledge the National Aeronautics and Space Administration, the Petroleum Research Foundation, administered by the American Chemical Society, and the U.S. Air Force Office of Scientific research (under Grant No. F49620-98-0116) for their support of this research. M.H.G. gratefully acknowledges the support from the Director, Office of Energy Research, Office of Basic Energy Sciences, Chemical Science Division of the U.S. Department of Energy under Contract No. DE-Aco3-76SF00098.

References and Notes

(1) Siegmann, K.; Sattler, K. *J. Chem. Phys*. **2000**, *112*, 698, and references therein.
(2) Leger, A.; Puget, J. L. *Astron. Astrophys*. **1984**, *137*, L5.
(3) Allamandola, L. J.; Tielens, A. G. G. M.; Barker, J. R. *Astrophys. J*. **1985**, *290*, L25.
(4) Russel, R.; Soifer, B.; Willner, W. *Astrophys. J*. **1977**, *217*, L149; **1987**, *220*, 568.
(5) Szczepanski, J.; Vala, M. *Nature* **1993**, *363*, 699.
(6) Joblin, C.; Tielens, A. G. G. M.; Geballe, T. R.; Wooden, D. H. *Astrophys. J*. **1996**, *460*, L119-L122.
(7) Andrews, L.; Friedman, R. S.; Kelsall, B. J. *J. Phys. Chem*. **1985**, *89*, 4016.
(8) Szczepanski, J.; Roser, D.; Personette, W.; Eyring, M.; Pellow, R.; Vala, M. *J. Phys. Chem*. **1992**, *96*, 7876.
(9) Szczepanski, J.; Vala, M.; Talbi, D.; Parisel, O.; Ellinger, Y. *J. Chem. Phys*. **1993**, *98*, 4494.
(10) Szczepanski, J.; Drawdy, J.; Wehlburg, C.; Vala, M. *Chem. Phys. Lett*. **1995**, *245*, 539.
(11) Hudgins, D. M.; Sandford, S. A.; Allamandola, L. J. *J. Phys. Chem*. **1994**, *98*, 4243.
(12) Hudgins, D. M.; Allamandola, L. J. *J. Phys. Chem*. **1995**, *99*, 3033.
(13) Halasinski, T. M.; Hudgins, D. M.; Salama, F.; Allamandola, L. J.; Bally, T. *J. Phys. Chem. A* **2000**, *104*, 7484.
(14) Ekern, S. P.; Marshall, A. G.; Szczepanski, J.; Vala, M. *Astroph. J*. **1997**, *L39-L41*, 488.
(15) Ekern, S. P.; Marshall, A. G.; Szczepanski, J.; Vala, M. *J. Phys. Chem. A* **1998**, *102*, 3498.
(16) Dibben, M. J.; Kage, D.; Szczepanski, J.; Eyler, J. R.; Vala, M. *J. Phys. Chem. A* **2001**, *105*, 6024.
(17) Ho, Y. P.; Yang, Y. C.; Klippenstein, S. J.; Dunbar, R. C. *J. Phys. Chem*. **1995**, *99*, 12115.
(18) Maier, J. P.; Turner, D. W. *Discuss. Faraday Soc*. **1972**, *54*, 149.
(19) Schmidt, W. *J. Chem. Phys*. **1977**, *66*, 828.
(20) Oomens, J.; van Roji, A. J. A.; Meijer, G.; van Helden, G. *Astrophys. J*. **2000**, *542*, 404.
(21) Szczepanski, J.; Dibben, M. J.; Pearson, W.; Eyler, J. R.; Vala, M. *J. Phys. Chem. A* **2001**, *105*, 9388.
(22) Becke, A. D. *J. Chem. Phys*. **1993**, *98*, 5648.
(23) Foresman, J. B.; Head-Gordon, M.; Pople, J. A.; Frisch, M. J. *J. Phys. Chem*. **1992**, *96*, 135.
(24) Runge, E.; Gross, E. K. U. *Phys. Rev. Lett*. **1984**, *52*, 997.
(25) Casida, M. E. In *Recent Advances in Density Functional Methods, Part I*; Chong, D. P., Ed.; World Scientific: Singapore, 1995; p 155.
(26) Head-Gordon, M.; Rico, R. J.; Oumi, M.; Lee, T. J. *Chem. Phys. Lett*. **1994**, *219*, 21.
(27) Slater, J. C. *Quantum Theory of Molecules and Solids, Vol. 4: The Self-Consistent Field for Molecules and Solids*; McGraw-Hill: New York, 1974.
(28) Vosko, S. H.; Wilk, L.; Nusair, M. *Can. J. Phys*. **1980**, *58*, 1200, Parametrization 5.
(29) Becke, A. D. *Phys. Rev*. A **1988**, *38*, 3098.
(30) Lee, C.; Yang, W.; Parr, R. G. *Phys. Rev*. B **1988**, *37*, 785.
(31) Maurice, D.; Head-Gordon, M. *Int. J. Quantum Chem. Symp*. **1995**, *29*, 361.
(32) Maurice, D.; Head-Gordon, M. *J. Phys. Chem*. **1996**, *100*, 6131.
(33) Hirata, S.; Head-Gordon, M. *Chem. Phys. Lett*. **1999**, *302*, 375.
(34) Casida, M. E.; Jamorski, C.; Casida, K. C.; Salahub, D. R. *J. Chem. Phys*. **1998**, *108*, 4439.
(35) Tozer, D. J.; Handy, N. C. *J. Chem. Phys*. **1998**, *109*, 10180.

(36) Hirata, S.; Lee, T. J.; Head-Gordon, M. *J. Chem. Phys*. **1999**, *111*, 8904.
(37) Weisman, J. L.; Lee, T. J.; Head-Gordon, M. *Spectrochim. Acta, A* **2001**, *57*, 931.
(38) Bauernschmitt, R.; Ahlrichs, R. *Chem. Phys. Lett*. **1996**, *256*, 454.
(39) Jamorski, C.; Casida, M. E.; Salahub, D. R. *J. Chem. Phys*. **1996**, *104*, 5134.
(40) Stratmann, R. E.; Scuseria, G. E.; Frisch, M. J. *J. Chem. Phys*. **1998**, *109*, 8218.
(41) Hirata, S.; Head-Gordon, M. *Chem. Phys. Lett*. **1999**, *314*, 291.
(42) Geertsen, J.; Rittby, M.; Bartlett, R. J. *Chem. Phys. Lett.* **1989**, *164*, 57.
(43) Koch, H.; Jensen, Aa.; H. J.; Jørgensen, P.; Helgaker, T. *J. Chem. Phys*. **1990**, *93*, 3345.
(44) Rico, R. J.; Head-Gordon, M. *Chem. Phys. Lett*. **1993**, *213*, 224.
(45) Langhoff, S. R. *J. Phys. Chem*. **1996**, *100*, 2819.
(46) Bauschlicher, C. W. Jr. *Astrophys. J.* **1998**, *507*, L125- L127.
(47) Kong, J.; White, C. A.; Krylov, A. I.; et al. *J. Comput. Chem*. **2000**, *21*, 1532.
(48) Meerts, W. L.; Majewski, W. A.; van Herpen, W. M. *Can. J. Phys*. **1984**, *62*, 1293.
(49) Vala, M.; Szczepanski, J.; Pauzat, F.; Parisel, O.; Talbi, D.; Ellinger, Y. *J. Phys. Chem.* **1994**, *98*, 9187.
(50) Ruiščić, B.; Kovač, B.; Klasinc, L.; Güsten, H. *Z. Naturforsch*. **1978**, *33A*, 1006.
(51) Bally, T.; Carra, C.; Fülscher, M. P.; Zhu, Z. *J. Chem. Soc., Perkin Trans*. **1998**, *2*, 1759.
(52) Shida, T. *Electronic Absorption Spectra of Radical Ions*; Elsevier: New York, 1988; p 137.
(53) Bréchignac, P.; Pino, T.; Boudin, N. *Spectrochimica Acta, A* **2001**, *57*, 745.
(54) Pino, T.; Bréchignac, P.; Dartois, E.; Demyk, K.; d′Hendecourt, L. *Chem. Phys. Lett.* **2001**, *339*, 64.